RESEARCH ARTICLE

A combined view on precipitation and temperature climatology and trends in the southern Andes of Peru

Noemi Imfeld[1,2] | Katrin Sedlmeier[1,3] | Stefanie Gubler[1] |
Kris Correa Marrou[4] | Cristina P. Davila[4] | Adrian Huerta[4] |
Waldo Lavado-Casimiro[4] | Mario Rohrer[5,6] | Simon C. Scherrer[1] |
Cornelia Schwierz[1]

[1]Swiss Federal Office of Meteorology and Climatology, MeteoSwiss, Zurich, Switzerland

[2]Oeschger Centre for Climate Change Research and Institute of Geography, Bern, Switzerland

[3]Deutscher Wetterdienst, DWD, Munich, Germany

[4]Meteorological and Hydrological Service of Peru SENAMHI, Lima, Peru

[5]Meteodat GmbH, Zurich, Switzerland

[6]Climate Change Impacts and Risks in the Anthropocene (C-CIA), Institute for Environmental Sciences, University of Geneva, Switzerland

Correspondence
Noemi Imfeld, Institute of Geography, University of Berne Hallerstrasse 12, 3012 Bern, Switzerland.
Email: noemi.imfeld@giub.unibe.ch

Abstract

In the southern Peruvian Andes, communities are highly dependent on climatic conditions due to the mainly rain-fed agriculture and the importance of glaciers and snow melt as a freshwater resource. Longer-term trends and year-to-year variability of precipitation or temperature severely affect living conditions. This study evaluates seasonal precipitation and temperature climatologies and trends in the period 1965/66–2017/18 for the southern Peruvian Andes using quality-controlled and homogenized station data and new observational gridded data. In this region, precipitation exhibits a strong annual cycle with very dry winter months and most of the precipitation falling from spring to autumn. Spatially, a northeast–southwest gradient in austral spring is observed, related to an earlier start of the rainy season in the northeastern part of the study area. Seasonal variations of maximum temperature are weak with an annual maximum in austral spring, which is related to reduced cloud cover in austral spring compared to summer. On the contrary, minimum temperatures show larger seasonal variations, possibly enhanced through changes in longwave incoming radiation following the precipitation cycle. Precipitation trends since 1965 exhibit low spatial consistency except for austral summer, when in most of the study area increasing precipitation is observed, and in austral spring, when stations in the central-western region of the study area register decreasing precipitation. All seasonal and annual trends in maximum

temperature are larger than trends in minimum temperature. Maximum temperature exhibits strong trends in austral winter and spring, whereas minimum temperature trends are strongest in austral winter. We hypothesize, that these trends are related to precipitation changes, as decreasing (increasing) precipitation in spring (summer) may enhance maximum (minimum) temperature trends through changes in cloud cover. El Niño Southern Oscillation (ENSO), however, has modifying effects onto precipitation and temperature, and thereby leads to larger trends in maximum temperatures.

1 | INTRODUCTION

High-mountain regions are expected to be warming hotspots due to mechanisms such as decreasing snow albedo and surface-based feedbacks (Pepin *et al.*, 2015). For the central Andes, a warming trend of more than 0.2°C per decade has been observed in temperature records between 1981 and 2010, which is stronger than in coastal areas to the west of the mountains (Vuille *et al.*, 2015). The temperature trends have a clear dependence on elevation, with the strongest warming found at higher elevation as shown for land surface temperature from satellite data (Aguilar-Lome *et al.*, 2019). This elevation-dependence is also seen in station observations, but only for maximum temperature (Vicente-Serrano *et al.*, 2018). Minimum temperature shows a weaker warming at higher elevations. For the future, climate models project an intensified warming of 2–7°C until the end of the century depending on location and season (Urrutia and Vuille, 2009; Seiler *et al.*, 2013). Besides these ongoing and expected temperature increases, precipitation decreases have been projected until mid-century for the Central Andes (Minvielle and Garreaud, 2011; Neukom *et al.*, 2015). In high-mountain regions such as the southern Andes of Peru, temperature and precipitation changes have manifold significant effects on the livelihoods of people, for example, due to retreating glaciers (e.g., Salzmann *et al.*, 2013; Vuille *et al.*, 2018; Yarleque *et al.*, 2018) and decreasing snow cover which are important freshwater resources during the dry season (Buytaert *et al.*, 2017). Such changes affect the small-scale and rain-fed agriculture, which is the main source of income in the study area (Meteoswiss and Senamhi, 2020). Due to limited coping capacities, farmers are highly vulnerable to extreme events or climatic changes (e.g., Sietz *et al.*, 2012). A good understanding of the climate variability and of changes in the recent period is therefore

vital for regional adaptation policies and planning. Considering the importance of agriculture for the region, knowledge on the climate in the transition seasons, spring (September–October–November) and autumn (March–April–May) is especially important since precipitation and temperature in these seasons determine sowing dates as well as the length of the growing season.

The southern Peruvian Andes consist mainly of a plateau, with a mean elevation of 3,800 m situated at a climatic border, where the Andes act as a barrier between the year-round humid Amazon Basin in the east and the very dry Pacific coast in the west (Figure 1). On intra-annual scales, the climate of the region is characterized by a dry (May–October) and wet season (November–April), related to the position of zonal mid- and upper-level winds (Garreaud *et al.*, 2003; Garreaud, 2009). During the winter months (June–August), the subtropical jet stream is at its northernmost position and hinders regional moisture import from the Amazon region due to the prevailing westerly winds over the Altiplano (the highlands in Bolivia and partly in Peru), thus leading to dry conditions in the study area. Towards austral summer, the jet stream weakens and shifts southwards. At the same time, deep convection that is connected to the intertropical convergence zone (ITCZ) increases over the Amazon area. This change in the subtropical jet stream and the forming of the Bolivian High (due to latent heating from the Amazon and sensible heat release of the Andes) lead to increased easterly winds and moisture transport towards the Altiplano (Lenters and Cook, 1999; Vuille, 1999; Garreaud *et al.*, 2003), resulting in precipitation over the Altiplano region. Temperatures on the contrary, show only a weak annual cycle due to the low variations in solar irradiance throughout the course of the year with larger daily amplitudes than annual amplitudes (Hardy *et al.*, 1998).

On inter-annual time scales, the El Niño Southern Oscillation (ENSO) is known as the dominant feature leading to dry or wet years at the northern Peruvian coast

FIGURE 1 Topography and
station locations of the study area.
Stations symbols show the
availability of temperature or
precipitation data. The four regions
NW, CW, C and E are divided by thin
grey lines. The panel in the top right
corner shows the location of the
study area in South America. Lake
Titicaca is shown as lightblue
filled area
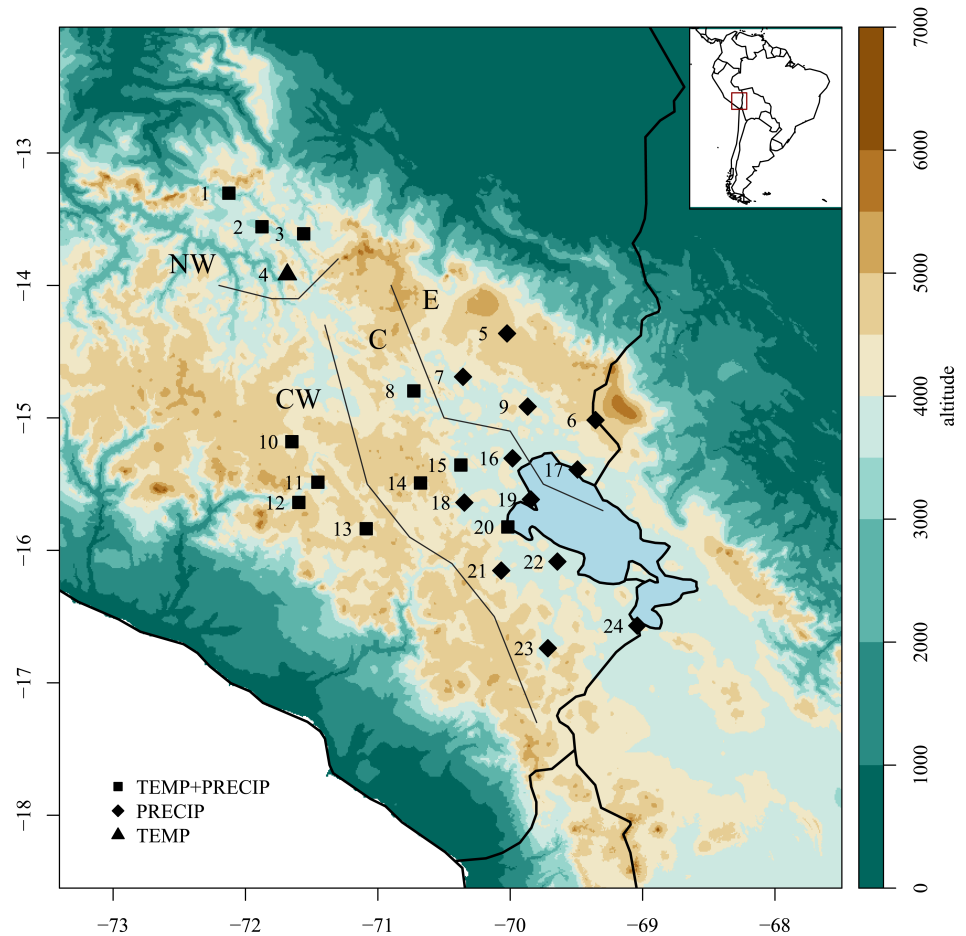
(Takahashi, 2004; Lagos *et al.*, 2008; Bazo *et al.*, 2013). This signal is opposite and less pronounced in the southern Andes of Peru. During El Niño, precipitation is reduced in the southern Andes (Vuille, 1999; Lavado Casimiro *et al.*, 2012) and dry spells are significantly more likely to occur (Sulca *et al.*, 2015; Huerta and Lavado-Casimiro, 2020), though the effect is not very pronounced. Temperature variability is more strongly modulated by ENSO and follows the sea surface temperature variations of the equatorial central Pacific with a lag of 1–2 months (Vuille *et al.*, 2000). Segura *et al.* (2016) show that on decadal to interdecadal timescales, hydrological deficits occur, that are related to the oscillation of central-western Pacific sea surface temperature and upper-level winds. For the northern Altiplano of Peru and Bolivia, including parts of our study area, Andrade (2018) provide a comprehensive overview of the mean climate and extremes of temperature and precipitation indices, describing the harsh climatic conditions. Analyses of annual mean temperature for the western South American Coast by Vuille *et al.* (2015), show a warming trend at higher elevations. Other studies report positive yearly temperature trends also for the Peruvian Andes during the last decades (Lavado Casimiro *et al.*, 2013; Salzmann *et al.*, 2013; Skansi

et al., 2013; Rosas *et al.*, 2016; Hunziker *et al.*, 2018) and seasonal temperature trends have been shown to be stronger in austral summer than winter (López-Moreno *et al.*, 2016). While for temperature existing trend analyses are coherent in space, precipitation trends are weak and show a high spatial variability. Haylock (2006) find decreasing annual precipitation and Salzmann *et al.* (2013) decreasing precipitation in all four seasons albeit low significance and considering only a single station in the study area and somewhat shorter periods. More recent studies based on a similar area find no spatially consistent trend pattern for annual data (Heidinger *et al.*, 2018) and the extended wet season (November–April) (Huerta and Lavado-Casimiro, 2020).

These previous studies focus on larger regions, considered only a few stations or specific time aggregations. A detailed view on the climate variability of all seasons looking at both temperature and precipitation and their interrelation has, however, not been performed for the southern Andes of Peru. A possible reason is the scarcity and quality of the available historical data in the region (Rosas *et al.*, 2016; Gubler *et al.*, 2017). In the course of the Climandes project, a cooperation project between the weather services of Switzerland and Peru (Rosas *et al.*, 2016), a carefully quality-controlled and homogenized

data set has been produced. Furthermore, gridded temperature and precipitation data sets have been generated by the Peruvian weather service and are available for the period since 1981 (Huerta *et al.*, 2018; Aybar *et al.*, 2019). These new data sets allow for a comprehensive analysis of the seasonal climatology and trends for both precipitation and temperature in the southern Peruvian Andes, which is presented in this study.

2 | DATA

2.1 | Station observations

The climate observations used in this study stem from manual station observations provided by the Peruvian weather service SENAMHI (Figure 1 and Table S1). For a period from 1965 to 2013, maximum and minimum temperature and precipitation time series were carefully selected, quality controlled, and homogenized (e.g., Gubler *et al.*, 2017) in the two projects Climandes (Rosas *et al.*, 2016) and DECADE (Hunziker *et al.*, 2017). For quality control, a standard quality control software (Zhang and Yang, 2004) in combination with a visual inspection has been used, as the data suffered from errors, which standard software often fails to detect (Hunziker *et al.*, 2017). Within the Climandes project, homogenization has been performed with the state-of-art, semi-automatic HOMER software (Mestre *et al.*, 2013), whereas within the DECADE project the fully automatic ACMANT method (Domonkos and Coll, 2017) has been applied. To provide an updated trend analysis, the homogenized time series have been extended with the most recent observations for the years 2014–2018. The data after 2013 is, thus, not homogenized, but we were not aware of any changes in stations and a visual inspection of the data did not reveal any breaks.

Not all of the stations considered in this study cover the full period since 1965. Hence, the climatological analysis is based on a total of 10 (11) stations for minimum (maximum) daily temperatures and 23 stations for daily precipitation sums, covering a standard 30 year climatological reference period from 1981/82 to 2010/11. The trend analysis is performed for the longer period from 1965/66 up to 2017/18, covering 53 years. Compared to the climatological analysis, the station network is thus somewhat reduced. For daily minimum (maximum) temperature, 10 (9) stations and for daily precipitation sums 21 stations are available (see Table S1).

2.2 | PISCO gridded dataset

For Peru, gridded datasets of daily precipitation and daily minimum and maximum temperature, PISCO (Peruvian

Interpolated data of SENAMHI'S Climatological and Hydrological Observations), are available since 1981 at a resolution of ~10 km × 10 km. These gridded datasets have recently been developed and are provided by the national weather and hydrological service of Peru (SENAMHI) and can be accessed online (http://iridl.ldeo.columbia.edu/SOURCES/.SENAMHI/.HSR/.PISCO/).

The gridded precipitation dataset PISCOp 2.1 is a blended product of three sources: quality-controlled and gap-filled station observations of precipitation, TRMM 2A25 satellite precipitation and CHIRP (Climate Hazards Group InfraRed Precipitation) gridded dataset (Aybar *et al.*, 2019). The generation involves a climatological correction of CHIRP on monthly scales using TRMM and station measurements. This product provides the basis for the daily and monthly merging of precipitation using Kriging and Inverse Distance Weighting, respectively. A monthly correction factor is added in order to provide higher spatial consistency to daily estimations and to ensure that the monthly aggregation of the daily product matches the monthly product. An independent validation and a comparison to the water balance evidence that the precipitation estimates are reasonable, but a more specific evaluation for the southern Andes of Peru is not yet available.

The gridded temperature dataset PISCOt1.1 includes minimum and maximum temperatures. It is based on quality-controlled, gap-filled, and homogenized station observations for minimum and maximum temperature, on surface temperature from the MODIS satellite and on a set of topographic predictors (Huerta *et al.*, 2018). The generation of the gridded product involves the estimation of a normal climate using weighted regression Kriging and the estimation of monthly and daily anomalies using regression splines. The two products are summed together leading to the final product. Cross-validation of PISCOt1.1 in the southern Peruvian Andes shows low mean absolute errors (MAE in the range of 0–0.5°C) and small biases that are close to zero for maximum temperatures. For minimum temperatures, the MAE are higher (up to 3°C) and the biases also show a larger range (−3 to +3°C).

In this study, the gridded data products are only used for a climatological description of the spatial variability of temperature and precipitation. Inhomogeneities inherent in the merged product impede its use for trend analyses.

2.3 | Study region

In order to facilitate a comparison between stations, the study area is subdivided into four regions based on

geographic features, the distance to the Amazon and topography (Figure 1). The four northern-most stations of the study area form the northwest region (NW) and lie at elevations between 3,070 and 3,690 m. The four western stations form the central-west region (CW) located at elevations between 3,660 and 4,450 m. The eastern region (E) contains the stations north and east of Lake Titicaca with elevations between 3,820 and 4,350 m. All other stations west and northwest of Lake Titicaca form the central region (C) located at elevations of around 3,900 m. These regions are compared against each other based on regional means calculated from the indices of each station.

3 | METHODS

3.1 | Climate analyses

Temperature and precipitation are analysed annually (June–May) and for the four seasons JJA (June–July–August), SON (September–October–November), DJF (December–January–February), MAM (March–April–May), covering the last climatological normal period from 1981 to 2010, for which station and gridded data both are available for the entire period. A year is defined starting in June and ending in May, as this best corresponds to the annual occurrence of the dry and wet season and to the ENSO cycle. Seasonal values are calculated accordingly: JJA 1981–2010, SON 1981–2010, DJF 1981/82–2010/11 and MAM 1982–2011. Climatologies are described by mean values for both station and gridded data. The mean is, however, only calculated when less than 20% of the values at a station or grid point are missing. To depict the seasonal differences for minimum and maximum temperature spatially, the temporal-mean seasonal anomalies with respect to the annual means are calculated.

Seasonal and annual trends are estimated for station data and for the regional-mean time series based on the longest available time period lasting from 1965/66 to 2017/18 and using the same definition of a year as described above. For continuous variables, a Theil-Sen slope estimator (Theil, 1950; Sen, 1968) is applied because it is more robust to outliers than ordinary linear regression and does not assume an underlying distribution of the data. The non-parametric Mann–Kendall test (Mann, 1945; Kendall, 1975) is used to test the significance of the trend at a 0.1 significance level (10%). Significant trends are marked, but non-significant trends are also discussed if they are spatially consistent, as they still may be relevant. For bounded count variables, such as frost days or dry days, logistic regression is used and trends are calculated based on the fitted trend line relative to the fitted value of the

year 1990 (i.e., the middle of the time series). In addition, trends are calculated with moving-windows for all possible periods within 1965/66–2017/18 covering at least 30 years in order to assess the sensitivity of trends regarding the selected period and whether they are related to some inter-annual to decadal variability.

Because ENSO may affect trends, a lagged regression is used for removing an ENSO-related part in the regional mean-time series of the indices (Werner et al., 2012). ENSO is described using the Southern Oscillation Index (SOI), calculated from the sea level pressure difference between Darwin and Tahiti (Ropelewski and Jones, 1987) and provided by the National Oceanic and Atmospheric Administration (NOAA). Instead of using a fixed amount of lags from the SOI, a stepwise backward regression is applied on every time series (i.e., on every season and region independently). To assess the impact of ENSO, trends are then calculated on the residual time series of the regression and compared to the trends of the original regional-mean time series.

Lastly, a correlation analysis between the different indices is preformed. To this end, the Pearson correlation is calculated for the different indices at station level using the full period 1965/66–2017/18. The correlation values are averaged for each region after applying a Fisher transformation to approximate a normal distribution (Wilks, 2011).

3.2 | Climate indices

The analyses focus on temperature and precipitation and four related indices from the list of indices defined by the Expert Team on Climate Change Detection (ETCCDI, http://etccdi.pacificclimate.org/, Table 1). In order to

TABLE 1 Definition of indices

Name	Definition	Unit
Precipitation indices		
Prcptot	Total precipitation sum	mm
RX5day	Maximum 5-day precipitation sum	mm
R10mm	Percentage of days with >10 mm rainfall	% days
Dry days	Percentage of days with ≤1 mm rainfall	% days
Temperature indices		
Mean t_{max}	Mean maximum temperature	°C
Mean t_{min}	Mean minimum temperature	°C
Frost days	Number of days with minimum temperature <0°C	% days

provide a general characterization of the climate of the study area, total precipitation (prcptot) and the mean of minimum temperature (t_{min}, often corresponding to nighttime temperature) and maximum temperature (t_{max}, often corresponding to daytime temperature) are analysed. In addition, an index describing precipitation frequency (R10mm, number of days with more than 10 mm rainfall), and one describing intensity (RX5day, maximum 5-day precipitation sum), the occurrence of dry days (DD), as well as the number of frost days (FD) are analysed. These additional indices are selected because of the thematic orientation of the Climandes project which focused on the agricultural sector.

In order to reduce the effect of missing data values on the index calculation, each index is only calculated if less than 20% of the values are missing during the aggregation period. Since total precipitation is more sensitive to missing values than the other indices, this index is only calculated if at most 10% of the data is missing. Indices counting the number of days (e.g., frost days or dry days) are expressed as a percentage with respect to the non-missing days in the respective aggregation period.

Depending on the index, the regional-mean time series are calculated following different approaches. For minimum and maximum temperature, the regional-mean time series are calculated as the mean of all stations' anomalies (with respect to the reference period 1981–2010) in one region. For total precipitation, a log-transformation is applied to the station time series in order to calculate the regional mean. For count variables (e.g., percentage of frost days), calculating a mean on the percentages leads to biased means. Thus, the data is shifted to −1 to 1 and a Fisher transformation is applied before calculating the mean. Because missing values also affect the calculation of the regional-mean time series, the missing values of the stations are replaced with the mean of the previous/following 5 years for minimum and maximum temperature and total precipitation.

All calculations are performed using the freely available R package ClimIndVis (www.github.com/Climandes/ClimIndVis). ClimIndVis allows for calculating indices for different temporal aggregations and includes a handling of missing values.

4 | RESULTS

4.1 | Precipitation climatology

In the southern Peruvian highlands, the long-term mean of total annual precipitation ranges from 441 to 837 mm for the different stations and is subject to a strong annual cycle (Figure 2a,b). In winter (JJA), total precipitation sums are very low with mean regional values of 11–19 mm, which corresponds bearly up to 3% of the mean annual precipitation sum (Figure 3a and Table 2). Climatologically, 66–81% of the total winter precipitation in the southern Peruvian Andes are accounted for by a mere 5-day precipitation period (Table S2). This corresponds to the fact that on average around 95% of the days are dry (∼85 out of 90 days), that is, receive less than 1 mm of precipitation. Considering stronger precipitation events, only every few winters a precipitation event of more than 10 mm (median R10mm <0.5%) is registered.

In spring (SON), when the transition from the dry to wet season happens, precipitation amounts increase in the whole study area, but with a considerable northeast–southwest gradient. Areas located closer to the Amazon (e.g., region E) obtain much more precipitation (143 mm) than western areas (e.g., region CW), which only receive around 54 mm (Figure 3b; note the different size of breaks in the colorbar). For the wetter areas, these amounts correspond to a fifth (21.3%) of the mean annual precipitation sum. In the drier areas (e.g., region CW), the precipitation falling in SON amounts to 9.8% of the mean annual precipitation sum and is also manifested in a higher amount of dry days (∼14 dry days more) in the drier area with a median of 89.3% of the days (Table 2 and Table S2). Precipitation sums, however, largely vary from year to year, especially in the drier CW region, standard deviation of precipitation sum is as high as the mean value (Table 2). The northeast–southwest pattern is also present in the maximum 5-day precipitation and in the number of rainy days above 10 mm.

Most precipitation falls in austral summer (DJF) with 314–388 mm, corresponding to 51.3–60.8% of total annual precipitation (Figure 3c, Table 2). The interannual variability is less pronounced than in SON with a standard deviation of around 30% of the mean value (Table 2). The highest precipitation amounts are recorded in hot-spots of the gridded dataset in the northwestern area, which are located at the eastern slopes of the mountain chain confining the plateau to the west. They could be related to orographic effects that lead to higher precipitation sums. In summer, it rains on average on half of the days with a dry day percentage of around 46–49.5% (Figure 3o and Table S2) and an average wet spell length of 2–4 days. The amount of dry days anti-correlates very well with the total precipitation sums. The Pearson correlation coefficients range between −0.72 and −0.94 in region NW, CW and C and are slightly lower in region E (−0.49 and −0.87). Also, the most frequent and intense precipitation events of the year occur in summer. The maximum 5-day precipitation totals increase to 55–71 mm on average (Table S2). This corresponds to around 18% of the total summer
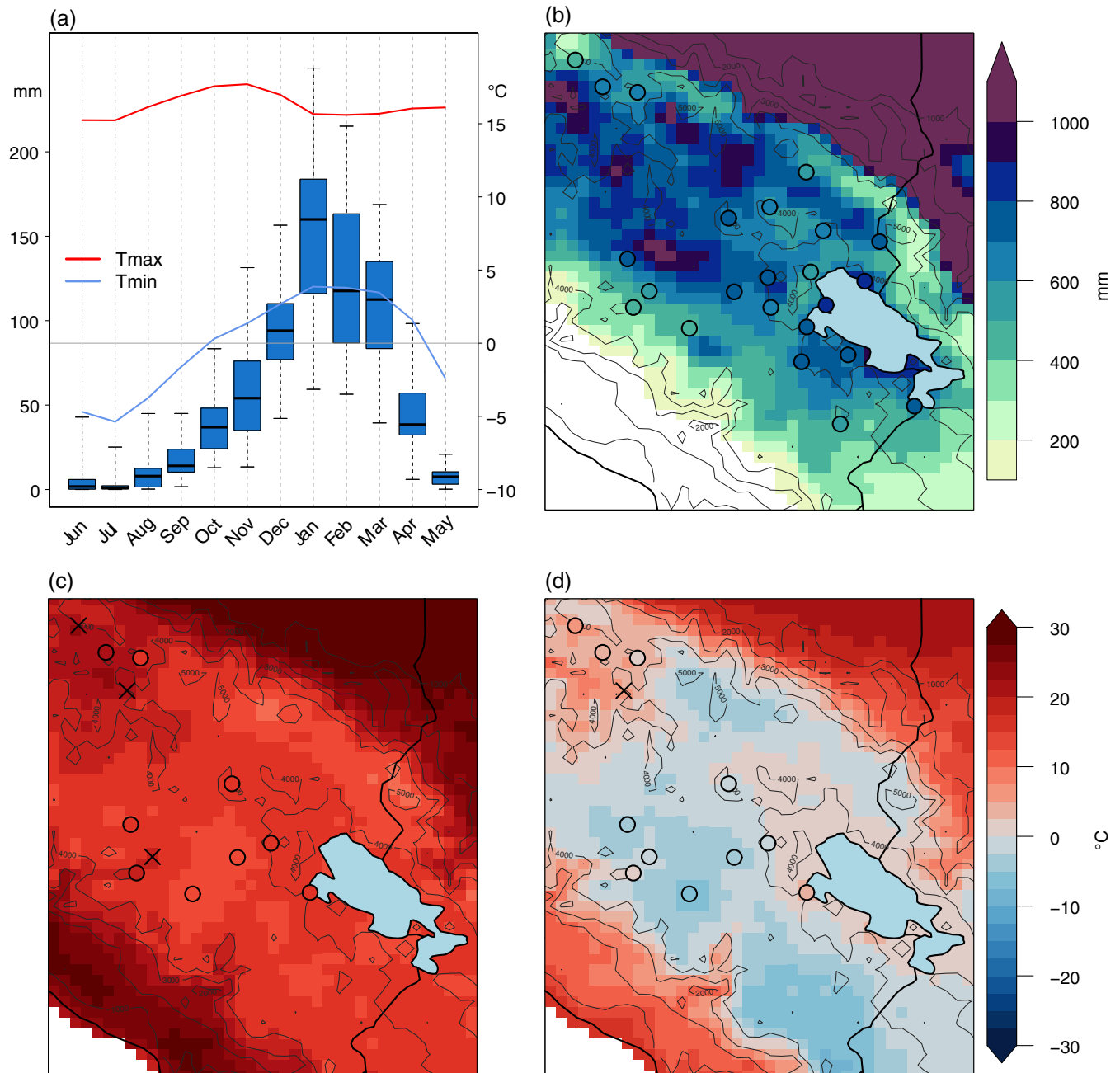
FIGURE 2 (a) Climate diagram of mean monthly values based on stations where both temperature and precipitation data are available. Temperature axis is to the right and precipitation to the left. Whiskers extend to the most extreme precipitation sums. (b) Mean of annual total precipitation, (c) mean of annual maximum temperature, and d) mean of annual minimum temperature for stations and gridded data. Coloured circles represent station measurements. All graphs are based on the period 1981–2010. Black crosses denote stations, where no mean has been calculated because more than 20% of daily values were missing. Lake Titicaca is shown as lightblue filled area and the elevation as grey contour lines

precipitation. The amount of precipitation events with more than 10 mm increases with a median of 11.3–15.9% days (Table S2).

The transition from the wet to the dry season takes place in austral autumn (MAM). During these months, precipitation sums in the study area decrease to 121–166 mm, corresponding to 21.5–25.9% of total annual precipitation (Figure 3d, Table 2). In contrast to the other transition season (SON), no southwest–northeast gradient of precipitation is seen. Dry days range between 72.1 and 76.8% days and are hence slightly less frequent than in spring and 5-day precipitation events are more intense (36–51 mm, Table S2). Compared to spring slightly more events occur with daily precipitation lying above 10 mm
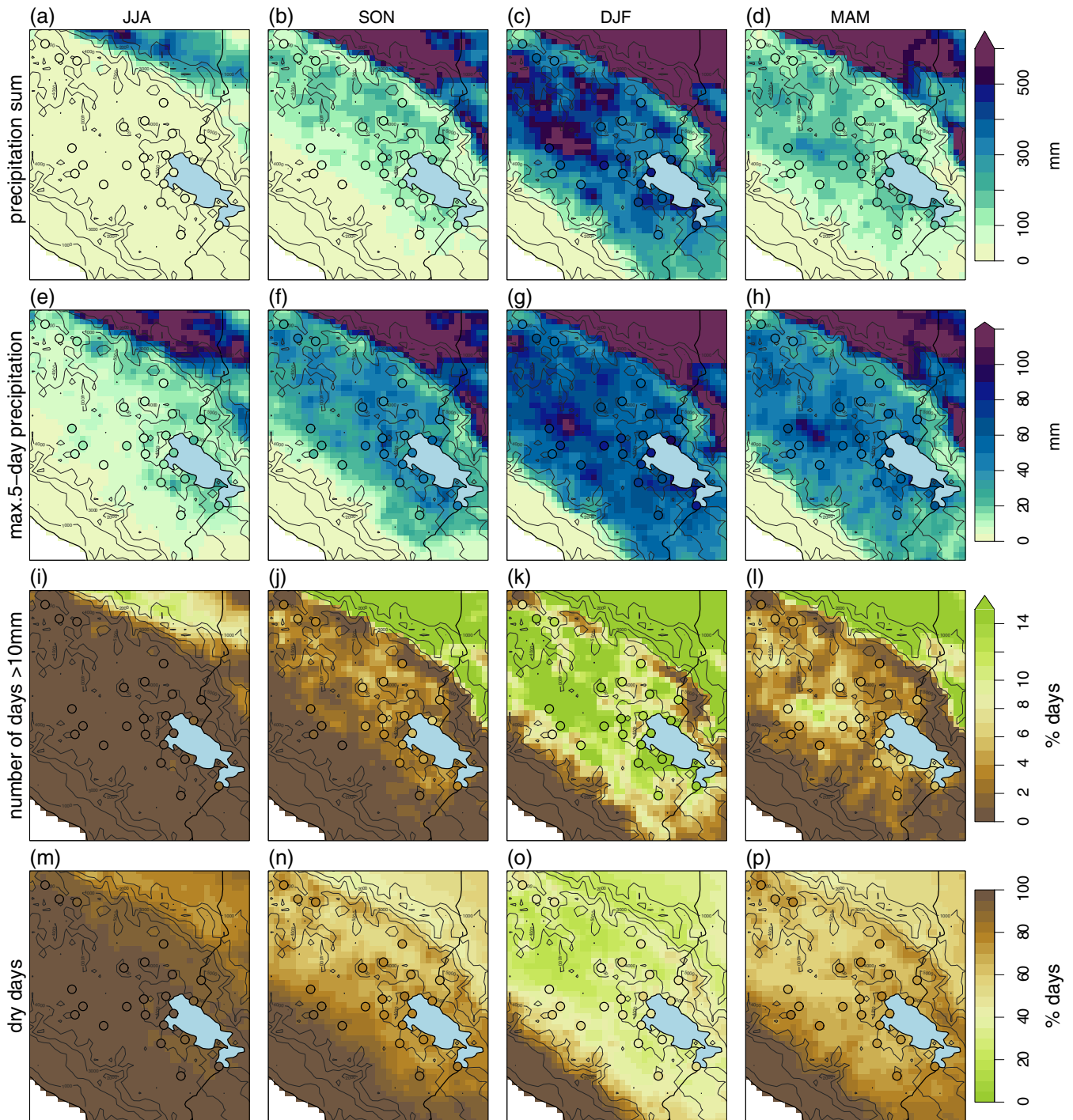
FIGURE 3 Seasonal means of precipitation indices for the period 1981–2010 for station data and gridded data. (a–d) Total precipitation sums, (e–h) maximum 5-day precipitation, (i–l) fraction of days above 10 mm and (m–p) fraction of dry days. Note the different scales on the colour tables. Coloured circle represent measurements. Lake Titicaca is shown as lightblue filled area and the elevation as grey contour lines

(3.7–5.8%, Table S2 and Figure 3p). The sub-seasonal variability between the different autumn months is, however, very high. The mean total precipitation of all stations is above 100 mm in March and decreases to below 15 mm in May (Figure 2a), and consequently, most dry days occur in April and May.

4.2 | Temperature climatology

The annual averages of daily maximum and minimum temperatures of the Peruvian Andes plateau stand out from the much warmer temperatures in the surrounding lower regions, that is, the Amazon and the coast

TABLE 2 Seasonal sums of total precipitation for the four regions NW, CW, C and E and the four seasons JJA, SON, DJF and MAM based on the regional-mean time series during the period 1981–2010

	JJA		SON		DJF		MAM	
	mm	**%**	**mm**	**%**	**mm**	**%**	**mm**	**%**
NW	15	2.7	113/29	20.0	314/64	55.7	121/42	21.5
CW	11	2.0	54/46	9.8	336/99	60.8	143/58	25.9
C	15	2.2	108/50	15.7	388/99	56.9	166/67	23.9
E	19	2.7	143/42	21.3	347/73	51.3	157/53	23.0

Note: The mean and standard deviation of seasonal total precipitation are shown in the first column of each season; the percentage contribution of each season to annual mean in the second column. For JJA, standard deviation of total precipitation is not shown, as the values are much larger than mean values.

TABLE 3 Mean maximum and minimum temperature for the three regions NW, CW and C and four seasons JJA, SON, DJF and MAM based on the regional time series during the period 1981–2010

	JJA		SON		DJF		MAM	
°C	T_{max}	T_{min}	T_{max}	T_{min}	T_{max}	T_{min}	T_{max}	T_{min}
NW	18.1	0.5	18.5	5.4	17.4	7.1	17.9	4.8
CW	15.3	−6.6	17.7	−2.7	16.3	1.6	16.0	−0.8
C	14.2	−5.9	16.3	−0.8	15.2	2.9	14.8	0.2

(Figure 2c,d). The highest annual and seasonal maximum and minimum temperatures are found in the area of the lower-lying NW stations. The annual cycles of maximum and minimum temperature differ considerably (Figure 2a). Maximum temperatures have only a weak annual cycle with differences in the order of 1.1–2.1°C between the seasons and with a peak in austral spring (SON) occurring in all regions. Lowest maximum temperatures are registered in austral winter (Figure 2a, Table 3 and Figure 4a–d). Interestingly, the seasonal anomaly is positive only during spring (SON) with anomalies up to 2°C, whereas for all other seasons the anomaly is slightly negative. Contrary to the maximum temperature, minimum temperature exhibits a more pronounced annual cycle (Figure 2a), with mean differences of 6.6–8.8°C between the seasons (Table 3). Lowest minimum temperatures occur in austral winter (JJA) when values below 0°C are prevalent. Consequently, the fraction of frost days is close to 100% in the whole region except for the lower-lying northwestern areas (Figure 4i–l, Table S2). In austral spring, the seasonal anomalies of minimum temperature (calculated with respect to the annual mean) are noteworthy: the northeastern areas are already about 1°C warmer than the annual average, whereas the southwestern areas are still up to 1.5°C colder than the annual average which may be related to the differences in cloud cover (Figure 4f). In austral summer (DJF), minimum temperatures are highest and lie between 1.6 and 2.9°C in region C and CW and at around 7.1°C in region NW (Table 3). Minimum temperatures in region C (CW) are thus close to 0°C even in summer and frost days occur on

average on 19.5% (29%—regional median) (Table S2). In the transition season spring (SON), the distribution of the frost day fraction for the regional mean of C ranges from 39.3 to 58.4% (interquantile range between the 10th and 90th percentile) and from 54.8 to 69.8% for region CW (Table S2). This variability corresponds to a mean minimum temperature in spring lying somewhat below 0°C (Table 3). Lake Titicaca exerts a marked warming effect on its surrounding areas during the cold and transition season. This can be seen for instance in the reduction of frost days near the lake compared to more distant locations (Figure 4j,l).

4.3 | Precipitation trends

The trends of the precipitation indices show a high spatial variability within the four different regions and for most of the seasons (Figure 5 and Figure S1). Spatially coherent trends are only seen in spring and summer. In spring, the CW region shows decreasing total precipitation, significant with a p-value smaller than 0.1 for one station. This tendency is also observed in the three other precipitation indices for the same region (Figure S1). The time series of the region CW, shows a non-significant trend (p value: 0.11) with a magnitude of −9.42% per decade, which corresponds to merely 4 mm per decade due to the low mean precipitation in spring in this region (Figure 6 and Table 4). In summer, total precipitation is increasing in most of the area except for several stations in region E (Figure 5). Strongest, positive, and mostly
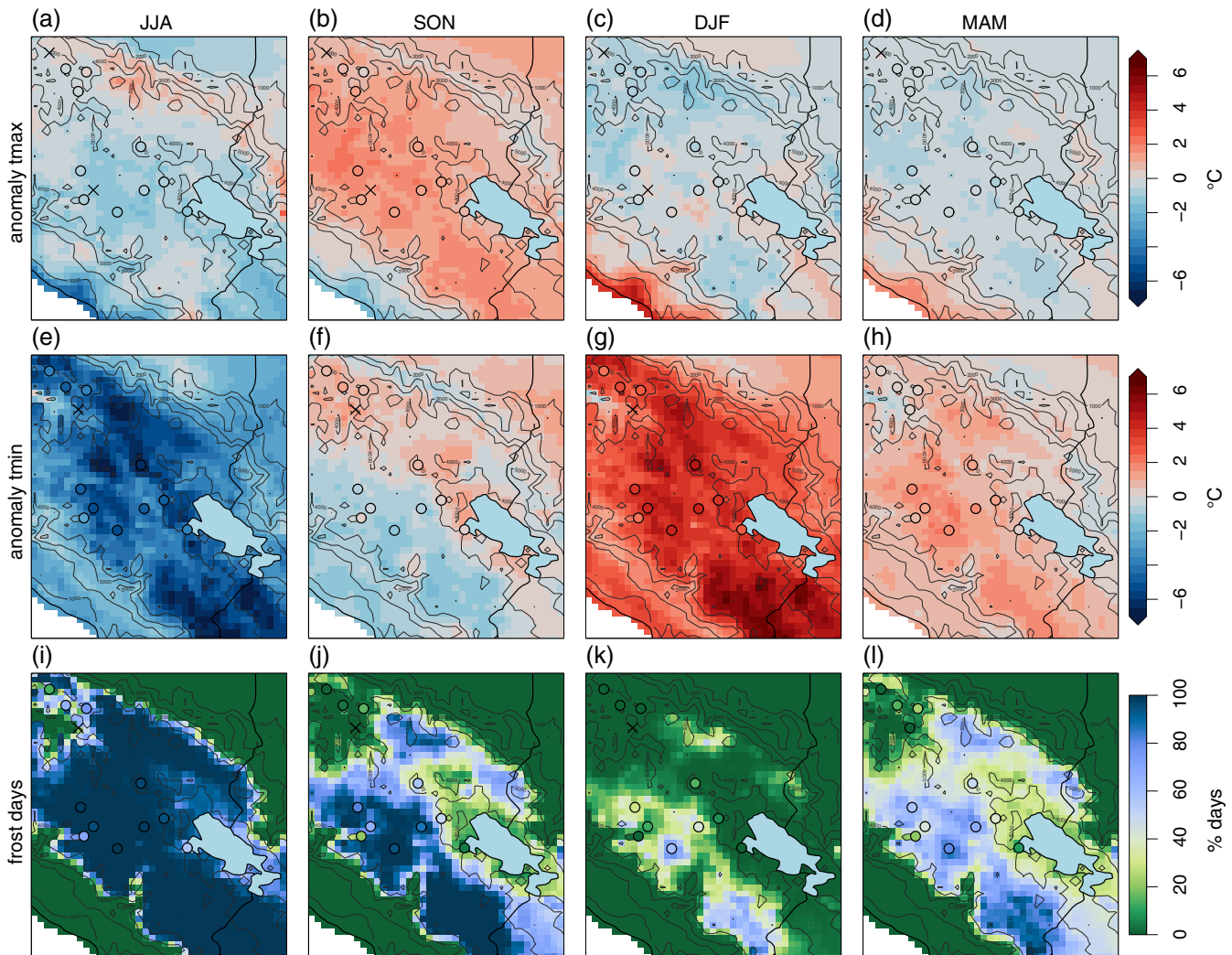
FIGURE 4 Seasonal temperature indices for the period 1981–2010 for station and gridded data. Minimum and maximum temperatures are shown as anomalies with respect to the 1981–2010 annual mean to highlight the seasonal differences. (a–d) Maximum temperatures, (e–h) minimum temperatures and (i–l) frost days. Coloured circles represent station measurements. Black crosses denote stations, where no mean has been calculated because more than 20% of daily values were missing. Lake Titicaca is shown as lightblue filled area and the elevation as grey contour lines

significant trends are found in region NW and CW, whereas towards the east, the trends weaken and even become non-significantly negative in the very east of the study area. For the region CW, the regional-mean time series for summer shows a non-significant positive trend with a magnitude of 4.13% per decade which corresponds to around 12 mm per decade (Figure 6). In region NW, the regional-mean time series has a significant trend with a magnitude of 6.3% per decade, whereas trends of the regional-mean time series from region C and E are non-significant negative (Table 4). The moving-window analysis from 1965/66 to 2017/18 shows that the negative spring and positive summer trends in total precipitation have been manifesting in the trends of shorter periods since 1970 (Figure S2). They are, thus, consistent in time

and not affected by the selection of time periods. Removing the ENSO-related signal from the time series of total precipitation has different effects depending on region and season. In summer, the total precipitation trend in the NW region becomes larger, whereas it becomes weaker for the regions CW and more negative for C and E (Table 4).

In accordance with total precipitation sums, both maximum 5-day precipitation sum and the number of events with more than 10 mm rainfall are increasing in summer in the majority of the study area, while the number of dry days is decreasing (Figure S1). The present analyses hence do not allow to attribute the increasing precipitations sums in DJF to either changes of intensity or frequency of precipitation, since both are increasing.
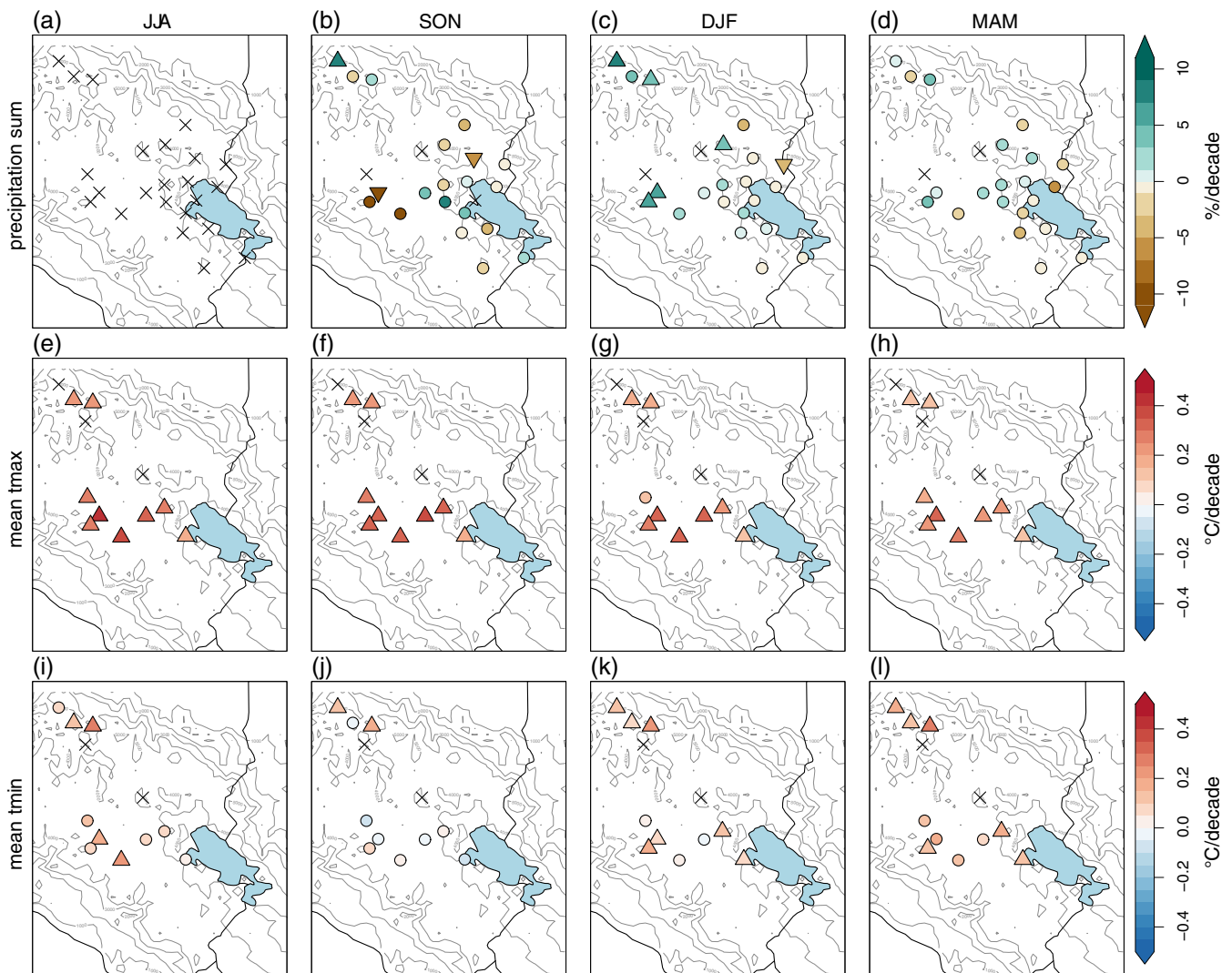
FIGURE 5   Trends for (a–d) total precipitation sum, (e–h) maximum temperature and (i–l) minimum temperature for the period 1965/66–2017/18 for station data only. Stations with trends significant at the 0.1 level are marked with an upward or downward triangle to denote positive and negative trends, respectively. When no trend could be calculated due to missing values, stations are marked with a black cross. Note that for total precipitation in JJA, no trends are calculated, because of the low amount of precipitation. Lake Titicaca is shown as lightblue filled area and the elevation as grey contour lines

In region E, where precipitation sums are slightly decreasing, the fraction of dry days is also decreasing. Histograms of the periods 1965–1990 and 1991–2017 for stations in region E show an increase in low precipitation events for the latter period, which explains these contrasting trends.

4.4 | Temperature trends

Trends of maximum temperature are spatially very consistent. All stations throughout all seasons show increasing and mostly significant trends with magnitudes ranging between 0.13 and 0.34°C per decade for the regional-mean time series (Figure 5e–h and Table 4). In all regions, trends

in maximum temperature are strongest in the drier seasons (winter and spring), compared to summer and autumn. Strongest trends of the regional mean are observed in the region CW (Table 4). In this region, the trend in annual maximum temperature is 0.27°C per decade (Figure 7) and the largest trend is observed in winter (0.34°C per decade). Spring (0.31°C per decade), autumn (0.25°C per decade) and summer (0.24°C per decade) show lower but still significant positive trends with p values below 0.01 (Figure 7). In spring and winter, after the year 2005, maximum temperatures mostly lie above the 1981–2010 mean. A noticeable feature are the striking positive temperature anomalies in summer and autumn, such as in 1982/83, 1997/98 or 2015/16, which are related to strong El Niño events (Figure 7d,e).
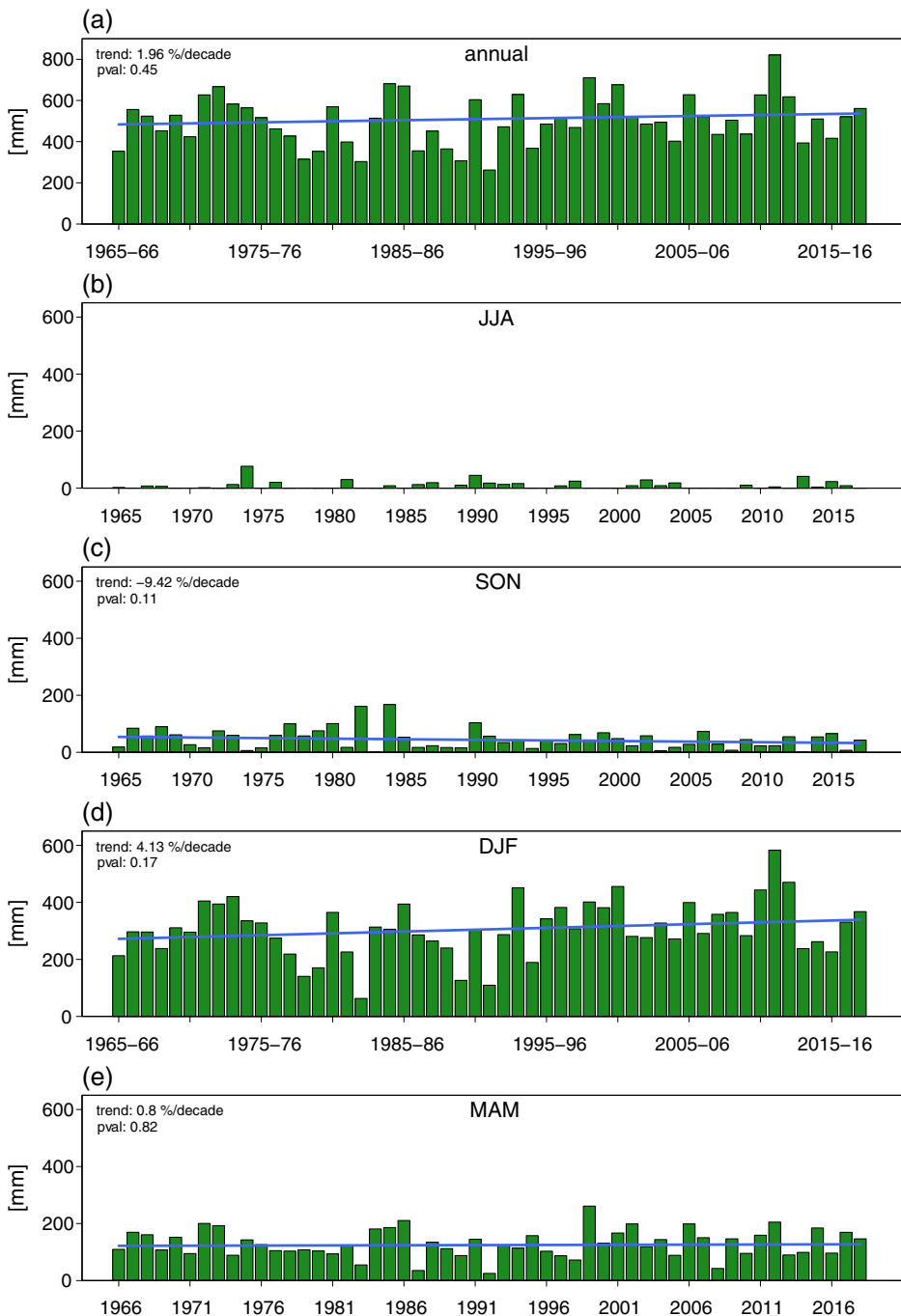
FIGURE 6 Time series of total precipitation for 1965/66–2017/18 for the station mean of the region CW. (a) Annual, (b) JJA, (c) SON, (d) DJF and (e) MAM. The blue line denotes the trend. Trend magnitudes and *p* values are noted in the upper left corner. Note that the *y*-axis is larger for the annual time series. For winter, JJA, no precipitation trends are shown, because the low precipitation sums can lead to high, but misleading relative trends. There are no missing values in the regional time series. If a bar is missing, this indicates that no or very little precipitation has been registered

The strong warming signal of day-time temperatures and the seasonal differences in the strength of the trends are also present in moving-windows analyses. In summer, also shorter episodes of weaker trends have been recorded (Figure S2). Removing the ENSO-related signal from the time series leads to weaker trends with differences of up to 0.16°C, but the trends are still significantly positive in the entire study area (Table 4). The largest reduction of trends owing to the removal of ENSO occur in austral winter, followed by austral spring, which are the seasons with largest trend magnitude in the original time series.

Trends of minimum temperature are spatially more variable and generally lower in magnitude compared to maximum temperature with magnitudes between −0.03 and 0.17°C per decade (Table 4 and Figure 5). Largest positive trends are registered in winter and autumn (0.16 and 0.12°C per decade), but only in winter they are statistically significant. In spring, no trend in minimum temperature is observed in region CW (Figure 7f–j). For frost days, trends mostly correspond to trends of minimum temperature with low magnitudes and few significant signals (Figure S1).

TABLE 4 Trends of regional time series for maximum and minimum temperature and total precipitation between 1965/6 and 2017/8 for the four seasons JJA, SON, DJF and MAM

	JJA			SON			DJF			MAM		
	T_{max}	T_{min}	Prcp	T_{max}	T_{min}	Prcp	T_{max}	T_{min}	Prcp	T_{max}	T_{min}	Prcp
NW												
1965/66–2017/18	*0.23*	*0.17*	—	*0.24*	*0.13*	3.21	*0.18*	*0.15*	*6.3*	*0.13*	*0.16*	1.54
No ENSO	*0.07*	*0.16*	—	*0.16*	*0.07*	2.97	*0.1*	*0.08*	*9.7*	*0.09*	*0.09*	−0.11
CW												
1965/66–2017/18	*0.34*	*0.16*	—	*0.31*	0	−9.42	*0.24*	*0.08*	4.13	*0.25*	0.12	0.8
No ENSO	*0.19*	0.06	—	*0.17*	0.01	−0.69	*0.17*	0.06	3.57	*0.15*	0.06	1.51
C												
1965/66–2017/18	*0.27*	0.07	—	*0.3*	−0.03	0.68	*0.2*	*0.06*	−0.18	*0.19*	0.11	0.28
No ENSO	*0.11*	0.04	—	*0.18*	−0.03	1.35	*0.11*	0.04	−2.26	*0.11*	0.01	−5.21
E												
1965/66–2017/18	—	—	—	—	—	−1.77	—	—	−1.40	—	—	−0.91
No ENSO	—	—	—	—	—	−4.25	—	—	−2.83	—	—	−3.4

Note: The lower row depicts trends, calculated on the residuals of a regression between the indices and SOI. Significant trends at the 0.1 level are shown in bold italics. Temperature trends are shown in °C/decade. Precipitation trends are calculated relative to the mean of the time series and shown as %/decade. For winter, JJA, no precipitation trends are shown, because the low precipitation sums can lead to high, but misleading relative trends.

In contrast to maximum temperature, the moving-window trend analysis shows, that minimum temperature trends have been much weaker for earlier periods and only started to become positive when looking at the most recent periods. For spring, most earlier periods in fact show negative trends, which become close to zero for the longest period from 1965/66 to 2017/18. Trends are, however, not significant throughout (Figure S2). Removing the ENSO-related signal from the time series leads to weaker trends of up to 0.1°C difference compared to the original trends depending on season and region (Table 4) and thus smaller effects compared to maximum temperature. For austral spring for example, trends are weaker only by up to 0.01°C.

4.5 | Correlation of pairs of indices

Correlations between maximum temperature and total precipitation are negative, lying between −0.34 and −0.59, with lowest values in autumn (Figure 8a). Minimum temperature and total precipitation, on the contrary, correlate positively between 0.45 and 0.66 for the four seasons, with the highest correlation occurring in spring. Likewise, frost days seem to coincide with low total precipitation sums, as indicated by the negative correlation values between −0.36 and −0.69 (Figure 8a). This behaviour is strongest in spring, when the transition from

the dry to the wet season occurs. The same behaviour is seen in the dry days index, which correlates positively (negatively) with maximum (minimum) temperature (Figure 8b). These correlations between precipitation and temperature indices stand in contrast to the lower correlation between minimum temperature and maximum temperature, which lie between −0.18 and −0.39 for the four seasons (Figure 8b). High maximum temperatures are thus occurring along with low minimum temperatures and low precipitation sums. The correlation analysis is, however, sensitive to the selected period, for example, correlations between minimum and maximum temperature become more negative (up to −0.5) for the shorter period 1981–2010.

5 | DISCUSSION

5.1 | The seasonal cycle of precipitation and temperature

Precipitation in the southern Andes of Peru exhibits a strong annual cycle, as has been shown by, for example, Garreaud (2009) and Lavado Casimiro *et al.* (2013). In all regions, the highest precipitation sums are observed in summer (on average 57% of annual sum) while winters are very dry (3% of annual sum). The high contribution of maximum 5-day precipitation to the seasonal sum in
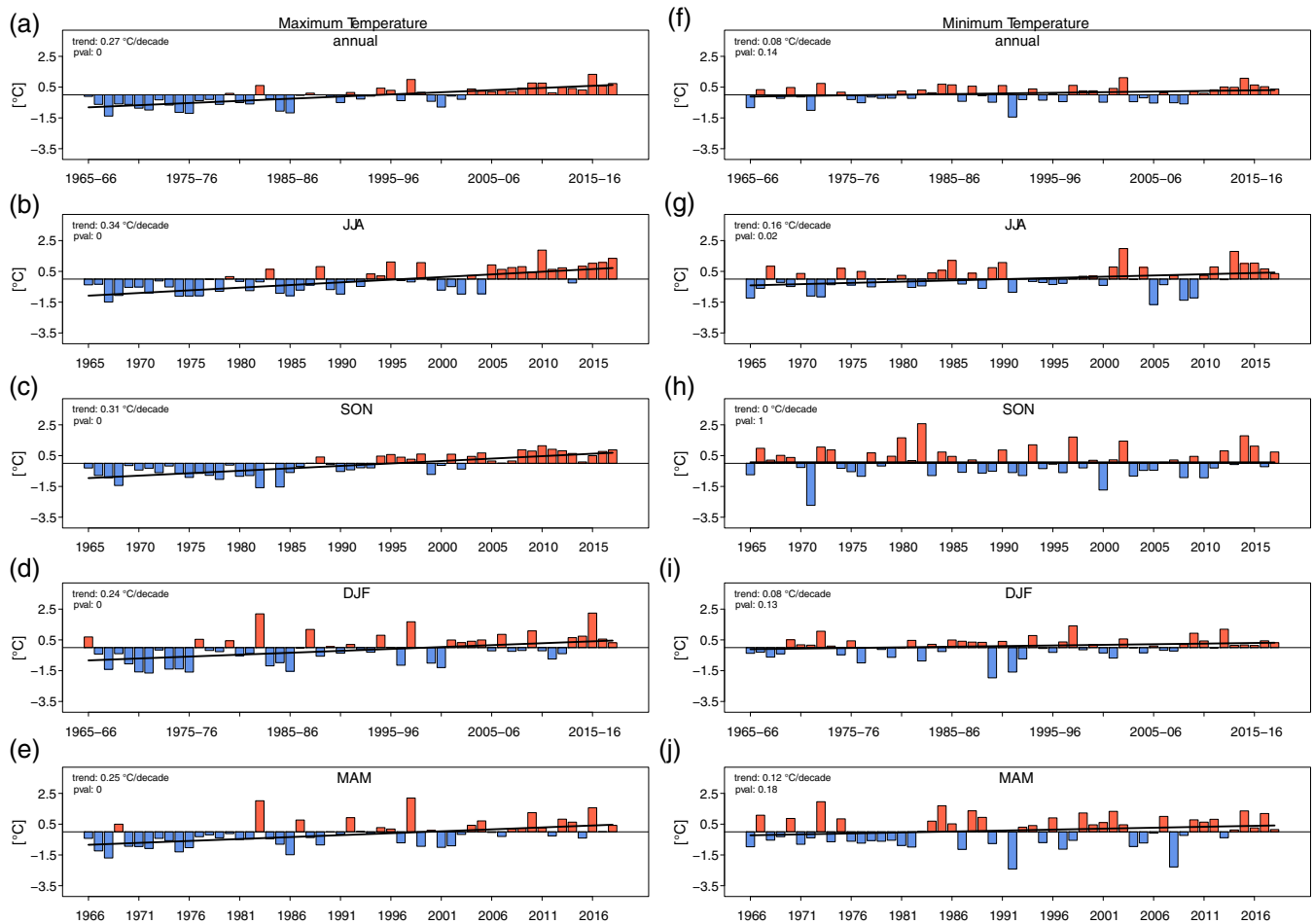
FIGURE 7 Time series of maximum and minimum temperature anomalies for 1965/66–2017/18 with respect to the 1981–2010 mean calculated for the regional time series of region CW. Left column shows maximum temperature, right column shows minimum temperature during (a, f) annual, (b, g) JJA, (c, h) SON, (d, i) DJF and (e, j) MAM. The black line denotes the trend. Trends in °C/decade and *p* values are shown in upper left corner. There are no missing values in the regional time series. If a bar is missing, this indicates that the temperature anomaly is very close to zero

winter suggests that most of the precipitation in the dry season actually falls within a few days. In contrast, during the wet summer season (DJF), the contribution of maximum 5-day precipitation to total precipitation is much lower (around 20%). In summer, precipitation is dominated by frequency rather than intensity (Huerta and Lavado-Casimiro, 2020), which is also confirmed by the high correlations of dry days and total precipitation observed in this study (Figure 8a). In austral spring (SON), precipitation is higher in northeastern than in southwestern areas as also shown by Andrade (2018), which may be related to the later start of the rainy season in the southwestern areas. Andrade (2018) further showed that the transition from dry to wet season happens within October to November, whereas the reverse transition from wet to dry takes place much faster within April only. This abrupt end of the rainy season is also seen in the annual precipitation cycle that drops close to zero around May (Figure 2a).

Temperature shows only moderate seasonal variations (up to 8.8°C for minimum and 2.4°C for maximum temperature) as extraterrestrial solar radiation varies less than 30% from winter to summer (Hastenrath, 1978; Hardy *et al.*, 1998; Garreaud *et al.*, 2003; Sicart *et al.*, 2016). Such variations are small compared to higher latitude variations, where seasonal differences can reach up to 20°C (e.g., Knutti *et al.*, 2006). Maximum temperature peaks in all regions in spring (Figures 2a and 4b) and not, as could be expected, in summer when incoming solar irradiance is highest. Andrade (2018) and Lavado-Casimiro *et al.* (2013) attributed this to less cloud coverage and hence stronger solar radiation in spring than in summer. In region NW, the lowest maximum temperature is indeed registered in summer, when the cloud cover is largest.

In contrast, minimum temperature reaches highest values in summer and lowest in winter corresponding to
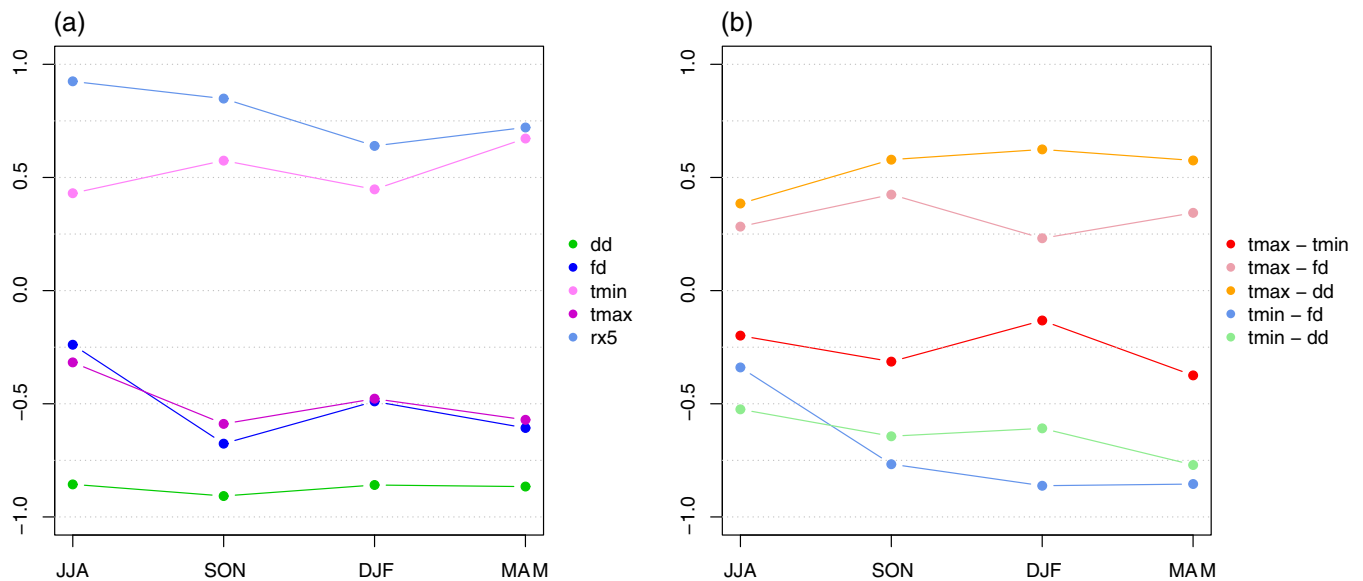
FIGURE 8 Mean Pearson correlation for different pairs of indices based on station time series in region CW and covering the full period from 1965/66 to 2017/18. (a) Correlation for total precipitation with dry days, frost days, minimum and maximum temperature and maximum 5-day precipitation. (b) Correlation between maximum and minimum temperature and with dry days, frost days

the annual changes of extraterrestrial solar radiation. The amplitude of the cycle of minimum temperature is higher than that of maximum temperature, likely because the minimum temperature cycle is amplified by the marked seasonality of incoming longwave radiation which itself is related to clouds through the enhancement of longwave emittance of the atmosphere in the wet period. Since frost days are strongly related to incoming longwave radiation (Garcia *et al.*, 2007), the occurrence of frost days follows the cycle of minimum temperature cycle. Regionally, difference in the occurrence of frost days are observed, for instance the percentage of frost days is considerably reduced close to the border of Lake Titicaca compared to the more distant areas. This indication of the warming effect of the lake on minimum temperature is more pronounced in the transition seasons SON and MAM when the mean minimum temperature is close to zero.

5.2 | Seasonal precipitation and temperature trends

For total precipitation, recent studies focusing on similar areas found few significant trends and a high spatial variability for both annual and extended wet season time series (November–April) for slightly different periods within 1964 and 2013 (Haylock, 2006; Skansi *et al.*, 2013; Heidinger *et al.*, 2018; Huerta and Lavado-Casimiro, 2020). Neukom *et al.* (2015) argued that the

long-term decreasing precipitation trend they observed comparing pre-industrial and present-day conditions may be superimposed by the spatial variability on the short period between 1965 and 2012. The east–west difference seen in summer precipitation trends (positive in the west and negative to the east of Lake Titicaca) was also observed by Huerta and Lavado-Casimiro (2020) for the extended wet season. However, the difference was less prominent since they concentrate their study on stations lying around Lake Titicaca. Based on principle components of the CHIRPS precipitation product, Segura *et al.* (2020) confirmed the significant increase in summer precipitation for the period 1982–2018, which is also found in the herein used longer period (and all other periods since 1970 covering at least 30 years). Segura *et al.* (2020) suggested that summer (DJF) precipitation is also associated to upward motion over the western Amazon, which has strengthened in the last decades, leading to a moistened mid-troposphere, decreased atmospheric stability and thus increased precipitation sums.

In agreement with previous studies on annual, seasonal, and monthly scales for similar regions (Seiler *et al.*, 2013; Sulca *et al.*, 2015; López-Moreno *et al.*, 2016; Rosas *et al.*, 2016; Hunziker *et al.*, 2018; Vicente-Serrano *et al.*, 2018), trends in maximum temperature (0.13–0.34°C/decade) are stronger than trends in minimum temperature (−0.03–0.17°C/decade). López-Moreno *et al.* (2016) suggested local factors and microclimate as an explanation for the weaker trends of minimum temperature.

The differences between the trends of maximum and minimum temperature, however, become smaller when removing the ENSO-related part of the temperature time series. ENSO leads to larger maximum temperature, but has less impact on minimum temperatures (e.g., Gubler *et al.*, 2020). When removing the ENSO signal, the strongest reduction in trend magnitude is found for winter maximum temperature. Winter maximum temperature correlates more strongly with ENSO at lags of 5–12 months (not shown). Hence, the previous ENSO cycle strongly influences winter maximum temperatures, which can be seen in the shifted peaks of winter maximum temperature anomalies compared to the El Niño peaks in summer (Figure 7b). The positive trends for maximum temperature thus are potentially amplified in all seasons by the more recent El Niño events that occurred in 2009/10, 2014/15 and 2015/16.

Comparing the magnitudes of temperature trends between the seasons, studies agree on stronger trends in winter than summer for maximum temperature and stronger trends in summer than winter for minimum temperature (Salzmann *et al.*, 2013; Seiler *et al.*, 2013; López-Moreno *et al.*, 2016). However, when the most recent years up to 2017/18 are included, the trends of minimum temperature become stronger in winter than in summer.

5.3 | Is precipitation modulating temperature through cloud cover?

The climatological descriptions of precipitation and temperature patterns and the trend analyses suggest that precipitation is modulating maximum as well as minimum temperatures through cloud coverage in time and space. Low precipitation sums are related to a low cloud coverage, which fosters higher maximum temperatures during the day (because of high incoming solar radiation) and lower minimum temperatures during the night (because of low incoming longwave radiation) and vice versa. For maximum temperature, such effects of cloud cover (and sunshine duration) have been reported for various areas of the world (Sun *et al.*, 2000; Xia, 2013; van den Besselaar *et al.*, 2015; Scherrer and Begert, 2019) and may be even more pronounced in high altitudes where the atmospheric transmissivity is large. For minimum temperature, the relation between cloud-free skies with low incoming longwave radiation and low temperature has been study in the Andes (Lhomme *et al.*, 2007; Saavedra and Takahashi, 2017). Further, its relation to the occurrence of frost days is well known (Garcia *et al.*, 2007).

In our case, this relationship gives an explanation to why highest maximum temperature is observed in spring

and not in summer. We also suggest that it is the reason for the larger amplitude in the annual cycle of minimum temperature compared to maximum temperature. The annual cycle of minimum temperature is likely amplified due to the marked seasonality of incoming longwave radiation due to clouds, that enhance the longwave emittance of the atmosphere. In addition, spatial effects of cloud cover on minimum temperature are visible. In spring, seasonal anomalies (calculated with respect to annual temperature) are lower in the southwestern region and higher in the northeastern region. This corresponds very well to the pattern of total precipitation (Figures 3b and 4f), that is, lower minimum temperatures occur in drier (and less cloudy) regions and higher minimum temperatures occur in wetter (and more cloudy) regions.

The same effects may provide a hitherto not discussed explanation for the different seasonal temperature trends. In the region CW, the decreasing precipitation potentially leads to the strong positive trends in maximum temperature (0.34°C per decade) compared to the annual trend. On the same time, the reduction in cloud cover counteract the trend in minimum temperatures (Figures 6 and 7). In summer, the positive precipitation trend goes along with a slightly weaker trend in maximum temperature compared to the annual trends whereas trends in minimum temperature are of the same magnitude as the annual trends. Another example provides the NW region in summer. The significant positive trend in precipitation potentially increases the trend in minimum temperature and lower the trend in maximum temperature, leading to very similar magnitudes. Pearson correlation further corroborates this hypothesis. Correlations for precipitation and minimum temperature are positive throughout the year, whereas they are negative for precipitation and maximum temperature, corresponding to the above described mechanism. The correlation coefficients for minimum and maximum temperature are, however, comparatively small.

This relation between temperature and precipitation should, however, not be seen as a concluding explanation, but as one likely contributing factor explaining spatio-temporal temperature patterns. More profound studies would be needed to determine the effect of cloud cover on temperature, along with possible other effects such as surface albedo and soil moisture.

6 | SUMMARY AND CONCLUSION

This study provides a detailed climatological description and trend analysis of maximum and minimum temperature, precipitation, and related indices for the southern

Peruvian Andes based on homogenized station data and newly available gridded data. It is the first study relating the spatio-temporal patterns of precipitation and temperature in this high mountain region. The region is known for a pronounced annual cycle of precipitation with a very dry winter and a wet summer. In spring, the transition from the dry to the wet season takes place, with substantial interannual variations and following a northeast–southwest gradient. Maximum temperature exhibits a weak annual cycle with the highest temperatures occurring in spring and small differences between the other seasons. Minimum temperature, on the contrary, shows a stronger annual cycle with a peak in summer and lowest values in winter following the annual cycle of solar radiation. Frost days occur in most of the study area year-round. In winter frost occurs almost every day, whereas in summer, frost days are less frequent but can still constitute around one-fifth of frost days in certain regions.

Precipitation trends for the period 1965/66–2017/18 exhibits low spatial consistency, except for austral summer, when a majority of stations show increasing precipitation. In austral spring, a consistent albeitnot significant signal of decreasing precipitation is found in the central-west region. Maximum temperature trends are sizeably stronger than minimum temperatures trends and exhibit considerable seasonal differences. Removing the ENSO-related signal from the regional-mean time series leads to weaker maximum temperature trends in all seasons and regions. For minimum temperature, the trends of the "ENSO-free" time series also become weaker compared to the original trends, but the differences are smaller than for maximum temperature, because ENSO has less influence on minimum temperature. For precipitation no consistent effect can be observed, when removing the ENSO-related signal.

The climatological description and trend analysis suggest that precipitation can influence minimum and maximum temperature through cloud cover. Three different effects of this relation have been observed:

1 We hypothesize that the annual minimum and maximum temperature cycles are modulated through the pronounced dry and wet seasons in the region. In general, the seasonal changes of the solar zenith determine temperature cycles. Therefore, the highest maximum temperature should be expected in summer when extraterrestrial incoming radiation is highest. Due to a pronounced cloud cover in summer, however, incoming solar radiation is reduced and maximum temperatures are not highest in summer but in spring. In contrast, annual changes in minimum temperature

correspond closer to changes in the solar zenith. We propose that the precipitation cycle might amplify the minimum temperature cycle due to radiative cooling in the dry season and increased incoming longwave radiation in the rainy season.

2 During the transition season spring, precipitation is higher in regions lying closer to the Amazon. This northeast–southwest pattern is also observed in the seasonal maximum and minimum temperature anomalies in spring. The maximum temperature is slightly reduced in the regions with high precipitation amounts, while in the same regions, the minimum temperature is higher.

3 The decreasing trend of precipitation in spring in region CW goes along with the strongest positive maximum temperature trend and no trend in minimum temperature. In summer, when precipitation has increased over the last 53 years, the maximum temperature trends are weaker compared to annual trends, whereas minimum temperature trends correspond to annual temperature trends. As argued above, we propose that the increasing (decreasing) precipitation and the related increase (reduction) in cloud cover in austral summer (spring) leads to a weaker (stronger) maximum temperature trend compared to the annual trend, and vice-versa for minimum temperatures.

This relation between precipitation and temperatures through cloud cover could be a relevant mechanism to understand seasonal temperature variability in the southern Peruvian Andes. Further studies may help to quantify these relations between cloud coverage and day- and nighttime temperature by the integration of cloud cover and radiation data into the analyses. However, for these variables high-quality and long-term data are scarce in the study area, emphasizing the need for well-developed monitoring networks and the importance of data rescue. Investigating the relation between temperature and precipitation is especially important as decreasing precipitation is predicted for the future (Minvielle and Garreaud, 2011; Neukom et al., 2015), and hence maximum temperatures might rise even more strongly having further implications on livelihoods of people, such as enhancing water scarcity.

ORCID

Noemi Imfeld https://orcid.org/0000-0002-9645-6875
Stefanie Gubler https://orcid.org/0000-0002-3733-953X
Adrian Huerta https://orcid.org/0000-0002-2415-3402
Waldo Lavado-Casimiro https://orcid.org/0000-0002-0051-0743
Simon C. Scherrer https://orcid.org/0000-0002-5040-0470

REFERENCES

Aguilar-Lome, J., Espinoza-Villar, R., Espinoza, J.C., Rojas-Acuña, J., Willems, B.L. and Leyva-Molina, W.M. (2019) Elevation-dependent warming of land surface temperatures in the Andes assessed using MODIS LST time series (2000–2017). *International Journal of Applied Earth Observation and Geoinformation*, 77(January), 119–128. https://doi.org/10.1016/j.jag.2018.12.013.

Andrade, M.F. (2018) Atlas - Clima y eventos extremos del Altiplano central Perú-boliviano / climate and extreme events from the central Altiplano of Peru and Bolivia 1981-2010. *Geographica Bernensia*, 188. https://doi.org/10.4480/GB2018.N01.

Aybar, C., Fernández, C., Huerta, A., Lavado, W., Vega, F. and Felipe-Obando, O. (2019) Construction of a high-resolution gridded rainfall dataset for Peru from 1981 to present day. *Hydrological Sciences Journal*, 0(0), 1. https://doi.org/10.1080/02626667.2019.1649411.

Bazo, J., Lorenzo, M.D.L.N. and Porfirio Da Rocha, R. (2013) Relationship between monthly rainfall in NW Peru and tropical sea surface temperature. *Advances in Meteorology*, 2013, 1–9. https://doi.org/10.1155/2013/152875.

van den Besselaar, E.J.M., Sanchez-Lorenz, A., Wild, M., Klein Tank, A.M.G. and de Laat, A.T.J. (2015) Relationship between sunshine duration and temperature trends across Europe since the second half of the twentieth century. *Journal of Geophysical Research*, 120(20), 10,823–10,836. https://doi.org/10.1002/2015JD023640.

Buytaert, W., Moulds, S., Acosta, L., De Bièvre, B., Olmos, C., Villacis, M., Tovar, C. and Verbist, K.M.J. (2017) Glacial melt content of water use in the tropical Andes. *Environmental Research Letters*, 12(11), 114014. https://doi.org/10.1088/1748-9326/aa926c.

Domonkos, P. and Coll, J. (2017) Homogenisation of temperature and precipitation time series with ACMANT3: method description and efficiency tests. *International Journal of Climatology*, 37(4), 1910–1921. https://doi.org/10.1002/joc.4822.

Garcia, M., Raes, D., Jacobsen, S.E. and Michel, T. (2007) Agroclimatic constraints for rainfed agriculture in the Bolivian Altiplano. *Journal of Arid Environments*, 71(1), 109–121. https://doi.org/10.1016/j.jaridenv.2007.02.005.

Garreaud, R.D. (2009) Advances in geosciences the Andes climate and weather. *Advances in Geosciences*, 7(1), 1–9. https://doi.org/10.5194/adgeo-22-3-2009.

Garreaud, R., Vuille, M. and Clement, A.C. (2003) The climate of the Altiplano: observed current conditions and mechanisms of past changes. *Palaeogeography, Palaeoclimatology, Palaeoecology*, 194(1–3), 5–22. https://doi.org/10.1016/S0031-0182(03)00269-4.

Gubler, S., Hunziker, S., Begert, M., Croci-Maspoli, M., Konzelmann, T., Brönnimann, S., Schwierz, C., Oria, C. and Rosas, G. (2017) The influence of station density on climate data homogenization. *International Journal of Climatology*, 37(13), 4670–4683. https://doi.org/10.1002/joc.5114.

Gubler, S., Sedlmeier, K., Bhend, J., Avalos, G., Coelho, C.A.S., Escajadillo, Y., Jacques-Coper, M., Martinez, R., Schwierz, C., de Skansi, M. and Spirig, C. (2020) Assessment of ECMWF SEAS5 seasonal forecast performance over South America. *Weather and Forecasting, (March)*, 35(2), 561–584. https://doi.org/10.1175/waf-d-19-0106.1.

Hardy, D.R., Vuille, M., Braun, G., Keimig, F. and Bradley, R.S. (1998) Annual and daily meteorological cycles at high altitude on a Tropical Mountain. *Bulletin of the American Meteorological Society*, 79(9), 1899–1913. https://doi.org/10.1175/1520-0477(1998)079<1899:AADMCA>2.0.CO;2.

Hastenrath, S. (1978) Heat-budget measurements on the Quelccaya ice cap, Peruvian Andes. *Journal of Glaciology*, 20(82), 85–96.

Haylock, M.R. (2006) Trends in total and extreme south American rainfall in 1960-2000 and links with sea surface temperature. *Journal of Climate*, 19(8), 1490–1512. https://doi.org/10.1175/JCLI3695.1.

Heidinger, H., Carvalho, L., Jones, C., Posadas, A. and Quiroz, R. (2018) A new assessment in total and extreme rainfall trends over central and southern Peruvian Andes during 1965–2010. *International Journal of Climatology*, 38(January), e998–e1015. https://doi.org/10.1002/joc.5427.

Huerta, A. and Lavado-Casimiro, W. (2020) Trends and variability of precipitation extremes in the Peruvian Altiplano for the period 1971-2013. *International Journal of Climatology*. https://doi.org/10.1002/joc.6635.

Huerta, A, Aybar, C and Lavado-Casimiro, W. (2018) PISCO temperature v.1.1. Lima-Perú.

Hunziker, S., Gubler, S., Calle, J., Moreno, I., Andrade, M., Velarde, F., Ticona, L., Carrasco, G., Castellón, Y., Oria, C., Croci-Maspoli, M., Konzelmann, T., Rohrer, M. and Brönnimann, S. (2017) Identifying, attributing, and overcoming common data quality issues of manned station observations. *International Journal of Climatology*, 37(11), 4131–4145. https://doi.org/10.1002/joc.5037.

Hunziker, S., Brönnimann, S., Calle, J., Moreno, I., Andrade, M., Ticona, L., Huerta, A. and Lavado-Casimiro, W. (2018) Effects of undetected data quality issues on climatological analyses. *Climate of the Past Copernicus GmbH*, 14(1), 1–20. https://doi.org/10.5194/cp-14-1-2018.

Kendall, M.G. (1975) *Rank Correlation Methods*. London: Griffin.

Knutti, R., Meehl, G.A., Allen, M.R. and Stainforth, D.A. (2006) Constraining climate sensitivity from the seasonal cycle in surface temperature. *Journal of Arid Environments*, 19, 4224–4233.

Lagos, P., Silva, Y., Nickl, E., Mosquera, K., Lagos, P., Silva, Y., Nickl, E. and El Ni, K.M. (2008) El Niño related precipitation variability in Peru. *Advances in Geosciences*, 14(3), 231–237.

Lavado Casimiro, W.S., Ronchail, J., Labat, D., Espinoza, J.C. and Guyot, J.L. (2012) Analyse de la pluie et de l'écoulement au Pérou (1969–2004): Bassins versants du Pacifique, du Lac Titicaca et de l'Amazone. *Hydrological Sciences Journal*, 57(4), 625–642. https://doi.org/10.1080/02626667.2012.672985.

Lavado Casimiro, W.S., Labat, D., Ronchail, J., Espinoza, J.C. and Guyot, J.L. (2013) Trends in rainfall and temperature in the

Peruvian Amazon-Andes basin over the last 40years (1965-2007). *Hydrological Processes*, 27(20), 2944–2957. https://doi.org/10.1002/hyp.9418.

Lenters, J.D. and Cook, K.H. (1999) Summertime precipitation variability over South America: role of the large-scale circulation. *Monthly Weather Review*, 127(3), 409–431. https://doi.org/10.1175/1520-0493(1999)127<0409:spvosa>2.0.co;2.

Lhomme, J.P., Vacher, J.J. and Rocheteau, A. (2007) Estimating downward long-wave radiation on the Andean Altiplano. *Agricultural and Forest Meteorology*, 145(3–4), 139–148. https://doi.org/10.1016/j.agrformet.2007.04.007.

López-Moreno, J.I., Morán-Tejeda, E., Vicente-Serrano, S.M., Bazo, J., Azorin-Molina, C., Revuelto, J., Sánchez-Lorenzo, A., Navarro-Serrano, F., Aguilar, E. and Chura, O. (2016) Recent temperature variability and change in the Altiplano of Bolivia and Peru. *International Journal of Climatology*, 36(4), 1773–1796. https://doi.org/10.1002/joc.4459.

Mann, H.B. (1945) Nonparametric tests against trend. *Econometrica*, 13(5), 245–259.

Mestre, O., Domonkos, P., Picard, F., Auer, I., Robin, S., Lebarbier, E., Böhm, R., Aguilar, E., Guijarro, J., Vertachnik, G., Klancar, M., Dubuisson, B. and Stepanek, P. (2013) HOMER: a homogenization software—methods and applications. *Idojaras*, 117(1), 47–67.

Minvielle, M. and Garreaud, R.D. (2011) Projecting rainfall changes over the south American Altiplano. *Journal of Climate*, 24(17), 4577–4583. https://doi.org/10.1175/JCLI-D-11-00051.1.

Neukom, R., Rohrer, M., Calanca, P., Salzmann, N., Huggel, C., Acuña, D., Christie, D.A. and Morales, M.S. (2015) Facing unprecedented drying of the Central Andes? Precipitation variability over the period AD 1000-2100. *Environmental Research Letters*, 10(8), 840 17. https://doi.org/10.1088/1748-9326/10/8/084017.

Pepin, N., Bradley, R.S., Diaz, H.F., Baraer, M., Caceres, E.B., Forsythe, N., Fowler, H., Greenwood, G., Hashmi, M.Z., Liu, X. D., Miller, J.R., Ning, L., Ohmura, A., Palazzi, E., Rangwala, I., Schöner, W., Severskiy, I., Shahgedanova, M., Wang, M.B., Williamson, S.N. and Yang, D.Q. (2015) Elevation-dependent warming in mountain regions of the world. *Nature Climate Change*, 5(5), 424–430. https://doi.org/10.1038/nclimate2563.

Ropelewski, C.F. and Jones, P.D. (1987) An extension of the Tahiti-Darwin southern oscillation index. *Monthly Weather Review*, 115, 2161–2165.

Rosas, G., Gubler, S., Oria, C., Acuña, D., Avalos, G., Begert, M., Castillo, E., Croci-Maspoli, M., Cubas, F., Dapozzo, M., Díaz, A., van Geijtenbeek, D., Jacques, M., Konzelmann, T., Lavado, W., Matos, A., Mauchle, F., Rohrer, M., Rossa, A., Scherrer, S.C., Valdez, M., Valverde, M., Villar, G. and Villegas, E. (2016) Towards implementing climate services in Peru—the project CLIMANDES. *Climate Services*, 4, 30–41. https://doi.org/10.1016/j.cliser.2016.10.001.

Rossa, A., Flubacher, M., Cristobal, L., Ramos, H. and Lechthaler, F. (2020) Towards more resilient food systems for smallholder farmers in the peruvian altiplano: the potential of community-based climate services. In: *Handbook of Climate Services*. Cham: Springer, 327–351. https://doi.org/10.1007/978-3-030-36875-3_17.

Saavedra, M. and Takahashi, K. (2017) Physical controls on frost events in the Central Andes of Peru using in situ observations and energy flux models. *Agricultural and Forest Meteorology*, 239, 58–70. https://doi.org/10.1016/j.agrformet.2017.02.019.

Salzmann, N., Huggel, C., Rohrer, M., Silverio, W., Mark, B.G., Burns, P. and Portocarrero, C. (2013) Glacier changes and climate trends derived from multiple sources in the data scarce cordillera Vilcanota region, southern Peruvian Andes. *The Cryosphere*, 7(1), 103–118. https://doi.org/10.5194/tc-7-103-2013.

Scherrer, S.C. and Begert, M. (2019) Effects of large-scale atmospheric flow and sunshine duration on the evolution of minimum and maximum temperature in Switzerland. *Theoretical and Applied Climatology.*, 138, 227–235. https://doi.org/10.1007/s00704-019-02823-x.

Segura, H., Espinoza, J.C., Junquas, C. and Takahashi, K. (2016) Evidencing decadal and interdecadal hydroclimatic variability over the Central Andes. *Environmental Research Letters*, 11(9), 094016. https://doi.org/10.1088/1748-9326/11/9/094016.

Segura, H., Espinoza, J.C., Junquas, C., Lebel, T., Vuille, M. and Garreaud, R. (2020) Recent changes in the precipitation-driving processes over the southern tropical Andes/western Amazon. *Climate Dynamics*, 54(5), 2613–2631. https://doi.org/10.1007/s00382-020-05132-6.

Seiler, C., Hutjes, R.W.A. and Kabat, P. (2013) Climate variability and trends in Bolivia. *Journal of Applied Meteorology and Climatology*, 52(1), 130–146. https://doi.org/10.1175/JAMC-D-12-0105.1.

Sen, P.K. (1968) Estimates of the Regression Coefficient Based on Kendall's Tau. *Journal of the American Statistical Association*, 63(324), 1379–1389.

Sicart, J.E., Espinoza, J.C., Quéno, L. and Medina, M. (2016) Radiative properties of clouds over a tropical Bolivian glacier: seasonal variations and relationship with regional atmospheric circulation. *International Journal of Climatology*, 36(8), 3116–3128. https://doi.org/10.1002/joc.4540.

Sietz, D., Choque, S.E.M. and Lüdeke, M.K.B. (2012) Typical patterns of smallholder vulnerability to weather extremes with regard to food security in the Peruvian Altiplano. *Regional Environmental Change*, 12(3), 489–505. https://doi.org/10.1007/s10113-011-0246-5.

Skansi, M., De los, M., Brunet, M., Sigró, J., Aguilar, E., Arevalo Groening, J.A., Bentancur, O.J., Castellón Geier, Y.R., Correa Amaya, R.L., Jácome, H., Malheiros Ramos, A., Oria Rojas, C., Pasten, A.M., Sallons Mitro, S., Villaroel Jiménez, C., Martínez, R., Alexander, L.V. and Jones, P.D. (2013) Warming and wetting signals emerging from analysis of changes in climate extreme indices over South America. *Global and Planetary Change*, 100, 295–307. https://doi.org/10.1016/j.gloplacha.2012.11.004.

Sulca, J., Vuille, M., Silva, Y. and Takahashi, K. (2015) Teleconnections between the Peruvian Central Andes and Northeast Brazil during extreme rainfall events in austral summer. *Journal of Hydrometeorology*, 17(2), 499–515. https://doi.org/10.1175/jhm-d-15-0034.1.

Sun, B., Groisman, P.Y., Bradley, R.S. and Keimig, F.T. (2000) Temporal changes in the observed relationship between cloud cover and surface air temperature. *Journal of Climate*, 13(24), 4341–4357. https://doi.org/10.1175/1520-0442(2000)013<4341:TCITOR>2.0.CO;2.

Takahashi, K. (2004) The atmospheric circulation associated with extreme rainfall events in Piura, Peru, during the 1997–1998 and 2002 El Niño events To cite this version: HAL Id: hal-00317738 Annales Geophysicae The atmospheric circulation associated with extreme rainf (January 1998), pp. 3917–3926.

Theil, H. (1950) A rank-invariant method of linear and polynomial regression analysis. *Nederl Akad Wetensch*, 386-392(521–525), 1397–1412.

Urrutia, R. and Vuille, M. (2009) Climate change projections for the tropical Andes using a regional climate model: temperature and precipitation simulations for the end of the 21st century. *Journal of Geophysical Research Atmospheres*, 114(2), 1–15. https://doi.org/10.1029/2008JD011021.

Vicente-Serrano, S.M., López-Moreno, J.I., Correa, K., Avalos, G., Bazo, J., Azorin-Molina, C., Domínguez-Castro, F., El Kenawy, A., Gimeno, L. and Nieto, R. (2018) Recent changes in monthly surface air temperature over Peru, 1964–2014. *International Journal of Climatology*, 38(1), 283–306. https://doi.org/10.1002/joc.5176.

Vuille, M. (1999) Atmospheric circulation over the Bolivian Altiplano during dry and wet periods and extreme phases of the southern oscillation. *International Journal of Climatology*, 19(14), 1579–1600. https://doi.org/10.1002/(SICI)1097-0088(19991130)19:14<1579::AID-JOC441>3.0.CO;2-N.

Vuille, M., Bradley, R.S. and Keimig, F. (2000) Climate variability in the Andes of Ecuador and its relation to tropical Pacific and Atlantic Sea surface temperature anomalies. *Journal of Climate*, 13(14), 2520–2535. https://doi.org/10.1175/1520-0442(2000)013<2520:CVITAO>2.0.CO;2.

Vuille, M., Franquist, E., Garreaud, R., Lavado Casimiro, W.S. and Cáceres, B. (2015) Impact of the global warming hiatus on Andean temperature. *Journal of Geophysical Research*, 120(9), 3745–3757. https://doi.org/10.1002/2015JD023126.

Vuille, M., Carey, M., Huggel, C., Buytaert, W., Rabatel, A., Jacobsen, D., Soruco, A., Villacis, M., Yarleque, C., Elison Timm, O., Condom, T., Salzmann, N. and Sicart, J.E. (2018) Rapid decline of snow and ice in the tropical Andes – impacts, uncertainties and challenges ahead. *Earth-Science Reviews*, 176(May 2017), 195–213. https://doi.org/10.1016/j.earscirev.2017.09.019.

Werner, A., Maharaj, A.M. and Holbrook, N.J. (2012) A new method for extracting the ENSO-independent Indian Ocean dipole: application to Australian region tropical cyclone counts. *Climate Dynamics*, 38(11–12), 2503–2511. https://doi.org/10.1007/s00382-011-1133-y.

Wilks, D.S. (2011) Chapter 5 - Frequentist statistical inference. *International Geophysics*, 100, 133–186. https://doi.org/10.1016/B978-0-12-385022-5.00005-1.

Xia, X. (2013) Variability and trend of diurnal temperature range in China and their relationship to total cloud cover and sunshine duration. *Annales Geophysicae*, 31(5), 795–804. https://doi.org/10.5194/angeo-31-795-2013.

Yarleque, C., Vuille, M., Hardy, D.R., Timm, O.E., De la Cruz, J., Ramos, H. and Rabatel, A. (2018) Projections of the future disappearance of the Quelccaya ice cap in the Central Andes. *Scientific Reports*, 8(1), 1–11. https://doi.org/10.1038/s41598-018-33698-z.

Zhang, X. and Yang, F. (2004) *RClimDex (1.0) User Manual*. p. 23.

SUPPORTING INFORMATION

Additional supporting information may be found online in the Supporting Information section at the end of this article.